Observation of a Field-Driven Structural Phase Transition in the Flux Line Lattice in $ErNi_2B_2C$

M. R. Eskildsen,[1] P. L. Gammel,[2] B. P. Barber,[2] U. Yaron,[2] A. P. Ramirez,[2] D. A. Huse,[2] D. J. Bishop,[2] C. Bolle,[3]
C. M. Lieber,[3] S. Oxx,[4] S. Sridhar,[4] N. H. Andersen,[1] K. Mortensen,[1] and P. C. Canfield[5]

[1]*Department of Solid State Physics, Risø National Laboratory, DK-4000 Roskilde, Denmark*
[2]*Bell Laboratories, Lucent Technologies, Murray Hill, New Jersey 07974*
[3]*Harvard University, Cambridge, Massachusetts 02138*
[4]*Northeastern University, Boston, Massachusetts 02115*
[5]*Iowa State University, Ames, Iowa 50011*

Small-angle neutron scattering and magnetic decoration both demonstrate a topological transition in the flux line lattice (FLL) in $ErNi_2B_2C$. The high-field square lattice slowly transforms into a hexagonal lattice via an area preserving [100] rhombohedral distortion below roughly 500 Oe. The square FLL is aligned with the [110] direction of the tetragonal crystal, while the two domains of the hexagonal FLL are aligned with [100] and [010]. The differences in pinning for the two FLL topologies are reflected in the rf kinetic inductance. [S0031-9007(97)02526-X]

PACS numbers: 74.60.Ge

The nominal incompatibility between superconducting and magnetic ground states requires that a system in which both occur develops novel strategies to allow microscopic coexistence. Studies of the magnetic ground states and their structures in such systems have, historically, prevailed [1]. Only recently has the flux line lattice (FLL) in these systems come under scrutiny despite the fact that all known materials in this class are strongly type-II superconductors which form a FLL in the mixed state.

Small-angle neutron scattering (SANS) studies [2] of the FLL in the magnetic superconductor $ErNi_2B_2C$ found a square FLL at high fields, contradictious to the hexagonal FLL typically found in strongly type-II superconductors. In this paper we report on SANS, magnetic decoration, and rf kinetic inductance studies which clearly show how the square FLL undergoes a smooth structural transformation to a hexagonal lattice below roughly 500 Oe at 3.5 K. The monodomain square lattice is aligned with the [110] direction of the host crystal, while the hexagonal lattice has domains aligned along [100] and [010]. This transformation proceeds via an area preserving rhombohedral distortion along the [100] axis.

Previous observations of FLL symmetry transformations were limited to the marginally type-II superconductor niobium in the intermediate mixed state, where a field independent transformation from a distorted hexagonal to a square lattice was seen by lowering the temperature [3,4].

Our experiments used single crystals of $ErNi_2B_2C$, grown using Ni_2B flux [5] and, to increase penetration of thermal neutrons, isotopically enriched B^{11}. Platelet samples, with the c axis perpendicular to the flat surface, were typically $8 \times 12 \times 1$ mm^3 with masses in the 300–500 mg range. $ErNi_2B_2C$ has a superconducting transition ($T_c = 10.5$ K) [5,6] and an antiferromagnetic transition ($T_n = 6.0$ K) [5,7,8]. It is a strongly type-II

superconductor, with $\kappa \sim 5$. Our experiments were performed in the antiferromagnetic superconducting regime.

The SANS experiments, performed at the cold neutron guide hall at Risø National Laboratory, employed magnetic fields between 200 and 3000 Oe applied parallel to both the c axis of the crystal (to within 4°) and the incident neutron beam. In this orientation, the upper critical field is $H_{c2}(2$ K$) = 1.8$ T [5] and there is no field dependence to T_n [5]. The neutrons had a wavelength, λ_n, between 9 and 15.3 Å, a wavelength spread $\Delta\lambda_n/\lambda_n = 18\%$, and angular divergences of $\sim 0.15°$ and $\sim 0.18°$ in the horizontal and vertical directions, respectively. An area detector at the end of a 6 m long evacuated chamber counted neutrons Bragg scattered from the magnetic field pattern due to the FLL.

Shown in Fig. 1 are SANS data as a function of applied field for a field cooled experiment. This figure shows the scattered intensity, after zero field background subtraction, in the plane of the detector at 3.5 K for 1000, 750, and 500 Oe. The data are shown for a single point on the rocking curves, centered relative to all four Bragg reflections. All the peaks remain essentially at the Bragg condition for this condition, since the rocking curve width is greater than the scattering angle. The data at high fields clearly show both the square symmetry of the FLL and its alignment with the [110] crystal direction [2]. In addition to the (10) peaks, the well ordered FLL shows strong (11) reflections. As the field is reduced, two effects are obvious. The first is the reduction in the scattering vector due to the field dependence of the flux line density. The second effect, the subject of this paper, is the azimuthal broadening which occurs as the field is reduced below 500 Oe. In contrast to the azimuthal width, the radial width remains roughly constant and resolution limited as the field is reduced. Further, broadening of the rocking curve is smooth and continuous through this region and is
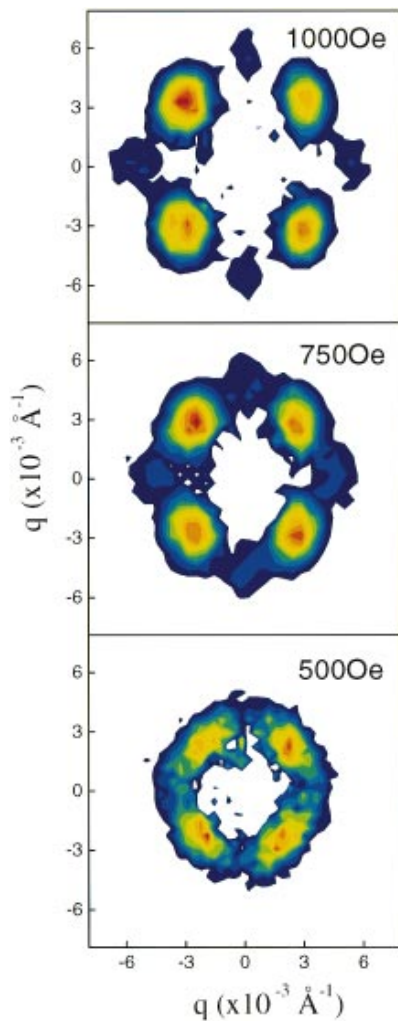
FIG. 1 (color). Two-dimensional contour maps of the background subtracted SANS intensity with $\mathbf{H} \parallel \mathbf{c}$ as a function of the scattering vector at 3.5 K.   The peaks undergo a pronounced azimuthal broadening at low field. The reduction in the scattering vector is due to the field dependence of the flux line density.

consistent with constant $J_c B$ and the Larkin-Ovchinnikov model [9]. The azimuthal broadening is the harbinger of the square to hexagonal transition. This broadening cannot be explained by a simple disordering of the FLL, which would lead to an isotropic broadening in the plane of the detector.

We also imaged the FLL at low fields using magnetic decoration, wherein iron particles are evaporated onto the sample surface at low temperatures [10]. The particles preferentially decorate regions where the flux lines exit the sample, and a SEM is used to image the particle and, hence, flux line locations. Shown in Fig. 2 are real space and Fourier transforms of magnetic decoration images at 4.2 K for fields of 100 and 600 Oe. At 100 Oe, and for other decorations down to 20 Oe, the well ordered, hexagonal lattice is aligned with either the [100] or the [010] crystallographic directions. Frequently, large

domains of both orientations are observed. At 600 Oe the decorations show co-existing square and hexagonal lattices, with only short range correlations for either polytype. This field, the upper limit for our decorations, is still in the middle of the transition region between hexagonal and square lattices. In Fig. 2 a predominately square symmetric region is shown. The square lattice is aligned with the [110] direction, as in the SANS data.

Figure 3 shows the analysis of the SANS data. In the upper panel, results of Gaussian fits to the radial positions of the peaks on the detector at the maximum of the rocking curve are shown as the open symbols, with circles and squares denoting the square (10) and (11) peaks, respectively. Full rocking curves analyzed by simulating a $\theta - 2\theta$ scan are shown as the solid symbols. With the reciprocal space locations of the Bragg peaks normalized by $q_0 = 2\pi(B/\phi_0)^{1/2}$, the (10) square lattice peak is at $q/q_0 = 1$ and the (11) peak is at $\sqrt{2}$. For a hexagonal lattice, the (10) peak is at $(2/\sqrt{3})^{1/2} = 1.07$. The data approaches the square lattice values above 1 kOe. This plot emphasizes that the square lattice (11) peaks move in and (10) peaks move out, forming the (10) peaks for the hexagonal lattice as the field is reduced.

The lower panel of Fig. 3 shows the field dependence of the azimuthal width of the (10) peaks of the square lattice. As the field is reduced below 600 Oe, the peaks broaden substantially. The thin solid line is the experimental resolution function. The limited resolution of the SANS experiment obscures the twelve peaks of the two hexagonal domains at low fields, leaving only a modulated ring of scattering as the azimuthal width increases. The data in Fig. 3 suggest that the distortion from a square to a hexagonal FLL occurs smoothly over the range from 1100 to 350 Oe.

Sketched in the inset to Fig. 3 is the distortion between the two lattice symmetries. On the left is the reciprocal space description and on the right is the real space picture. The squares are square lattice points and the triangles are for the hexagonal lattice. The transformation proceeds via an area preserving, rhombohedral distortion along the crystalline [100] orientation. There are two equivalent distortions rotated by 90° with respect to each other. The two domains of the hexagonal lattice produce twelve equally spaced peaks. The square lattice would produce the four (10) peaks and the four (11) peaks found at high fields. The arrows show how the peaks evolve as the field is lowered. The four square lattice (10) peaks split in the azimuthal direction, and move out slightly to form eight of the twelve peaks for the hexagonal lattice. This splitting is the azimuthal broadening in the lower panel of Fig. 2. The square lattice (11) peaks also split, but in the radial direction. Four peaks move in to make a total of twelve hexagonal lattice peaks, and four peaks move out to form higher order peaks for the hexagonal lattice. However, due to the rapidly decreasing scattering intensity as a function of q, the higher order peaks are not observed. This decrease in intensity also gives rise to the
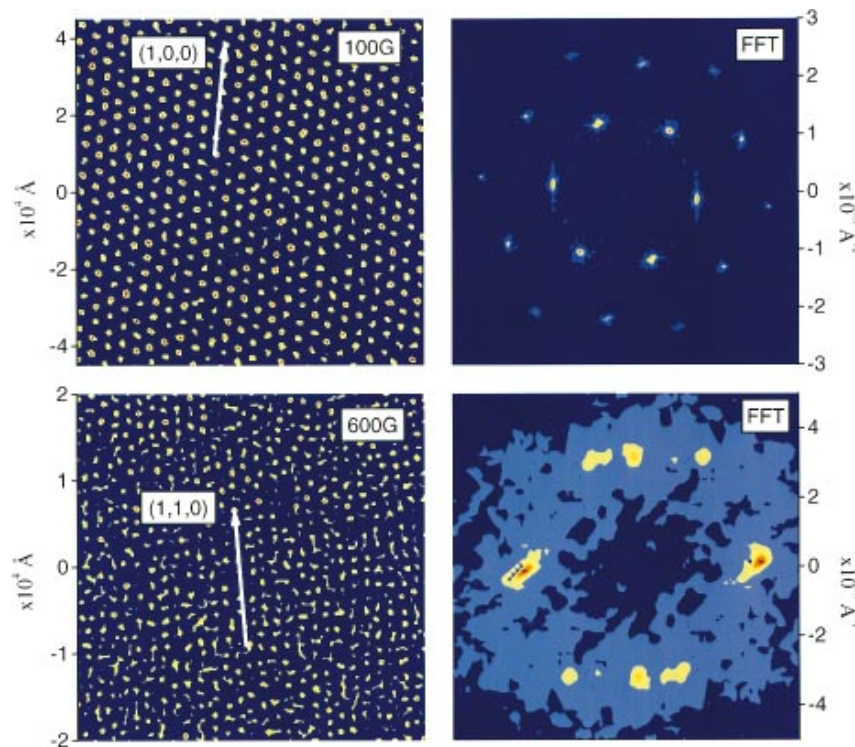
FIG. 2 (color).   Magnetic decoration images taken at 4.2 K.   Real space images are shown on the left and the Fourier transforms on the right. At 100 Oe, the well ordered hexagonal lattice is aligned in the [100] direction. At 600 Oe coexisting, disordered square and hexagonal lattices are seen. The square lattice, aligned with [110], dominates the region shown.

reduced intensity in the SANS data at 500 Oe in the direction of the square lattice (11) peaks.

It is also possible to argue for what drives the square to hexagonal transition. Within the family of lattices with rhombus-shaped unit cells, the high-field square lattice and the low-field hexagonal lattices are special cases. For an isotropic superconductor, the square lattice is a local maximum of the free energy and the hexagonal lattice is the global minimum, although the difference in energy between these is only about 2% of the condensation energy [11]. A small fourfold anisotropy, due, e.g., to H_{c2} anisotropy or magnetoelastic coupling, will select the two lowest free energy orientations of the hexagonal lattice, which differ by a 90° rotation. Increasing the fourfold anisotropy decreases the square lattice in energy relative to the two hexagonal ones, and it eventually becomes the global free energy minimum. The transition is continuous near H_{c2} in a model that includes Fermi surface anisotropy [12], although it could, in principle, be first order under other conditions.

We have studied a specific model for the FLL symmetry transition based on nonlocal corrections to the London model [13] valid in the regime of our experiments ($T \ll T_c$ and $H < H_{c2}$). This model accounts for the symmetry transition and the orientation of the FLL, as well as predicting that the transition field should increase with either increasing temperature, disorder, or tilt angle away from the c axis. The increase in transition field with temperature was seen at the qualitative level in the SANS data, although results at higher temperatures are not of sufficient S/N for a quantitative analysis.

Transport measurements [14] on single crystals of this compound have found a fourfold ab-plane anisotropy of H_{c2}, which increases dramatically below T_n. At 3.5 K, H_{c2} is 1.0 T along the [100] crystal direction and 1.3 T for the [110] direction. This anisotropy is well in excess of the 4% anisotropy required [12] to stabilize the square lattice at H_{c2}. The direct influence of the magnetic ground state on the FLL is through the enhanced H_{c2} anisotropy below T_n, which should stabilize the square FLL at lower fields than above T_n.

Since area is preserved in the transformation, it does not show up in $M(H)$ data with $\mathbf{H} \parallel \mathbf{c}$. However, the rf kinetic inductance, as measured in a tunnel diode oscillator apparatus, does show an effect. The sample, placed in the inductive coil of a tank circuit, changes the resonant frequency f, due to changes in the penetration depth λ. Using the relation $\Delta\lambda(T, H) = -g[f(T, H) - f_0(T, H)]$, where g is a geometrical factor, one can extract the temperature and field dependence of the penetration depth [15]. The extreme stability of the circuit, typically 1 Hz out of 3 MHz, allows penetration depth measurements with $o(\text{Å})$ resolution.

Shown as the solid line in Fig. 4 is $\Delta\lambda$ as a function of field for $T = 4.96$ K, $\mathbf{H} \parallel \mathbf{c}$, and $\mathbf{H}_{rf} \perp \mathbf{c}$. The rapid change in the flux penetration at $H_{c1} \sim 120$ Oe is clear. For this experimental configuration the vortex contribution to λ is given by $\lambda(H) = \mathrm{Re}\,[\phi_0 B(H)/\mu_0(\kappa_p - i\omega\eta)]^{1/2}$,
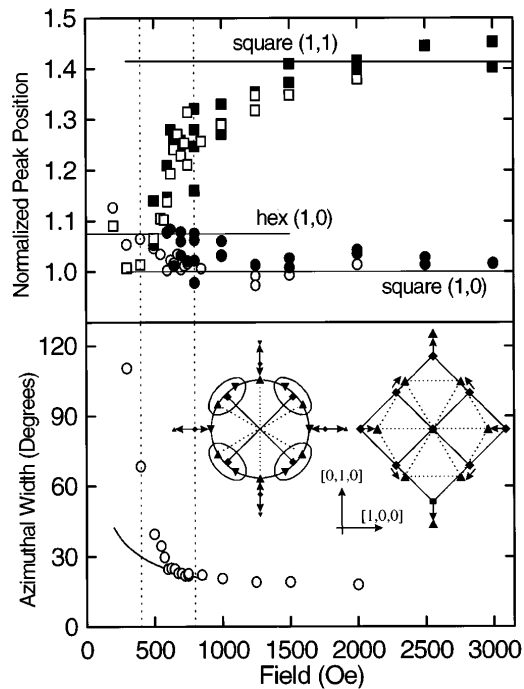
FIG. 3. The top panel shows the normalized positions of the FLL reflections. Open symbols are fits to the radial positions of the peaks on the detector at the peak of the rocking curve. Solid symbols are from simulated $\theta - 2\theta$ scans. Circles and squares represent positions of the (10) and (11) peaks, respectively. In the bottom panel are fits to the azimuthal widths of the square (10) peaks on the detector at the peak of the rocking curve, together with the experimental resolution function (line). Inset: schematic of the [100] rhombohedral distortion which transforms the square to the hexagonal FLL. The real space scenario is shown on the left and that in reciprocal space on the right. Hexagonal lattice points are the triangles, and square lattice points are the squares. The azimuthally broadened SANS peaks result from overlap of the circled peaks, shown on the left.

where $B(H)$ is the flux density in the sample, κ_p is an averaged pinning force constant, and η is the vortex viscosity. For uniform flux penetration $B(H) = H$, and the dominant
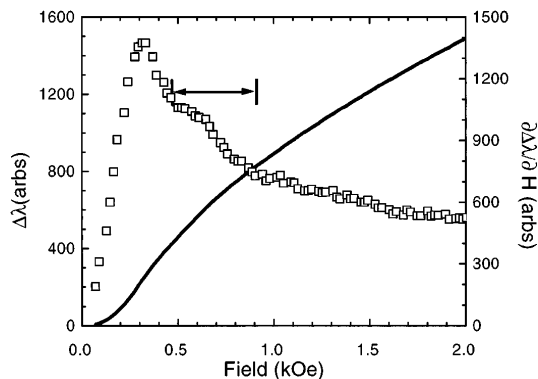
FIG. 4. Shown are the measured values of $\Delta\lambda$ as a function of field (line) and $d\lambda/dH$ versus field (squares) at $T = 4.96$ K. The arrow indicates the region of the square to hexagonal transition.

dependence is $\lambda \sim \sqrt{H}$. The vortex parameters κ_p and η are field independent, except in the vicinity of a phase transition.

The open symbols in Fig. 4 are the field derivative of the data, $d\lambda(H)/dH$. A feature is now clearly evident at $H \sim 600$ Oe, showing that the transport properties are also affected by the square to hexagonal transition. Changes in $\lambda(H)$ could be due to changes in $B(H)$, κ_p, or η. We believe the most likely candidate is κ_p, as at a FLL structural transition one would expect a change in the collective pinning properties of the lattice. Our data show the hexagonal and square lattices have different crystallographic orientations. This indicates that there is a sizeable pinning effect in this system, leading to a difference in κ_p for these two cases.

In conclusion, we have observed a square to hexagonal transition in the FLL symmetry of $ErNi_2B_2C$ using SANS, magnetic decoration, and rf kinetic inductance measurements. We find that the high-field square flux lattice is monodomain and aligned with the [110] direction of the crystal. Below roughly 500 Oe this gives way to a hexagonal lattice with two domains which are aligned with the [100] and [010] directions. The transition also causes changes in the rf kinetic inductance, presumably because the collective pinning properties of the lattice are influenced by its symmetry change.

[1] *Superconductivity in Magnetic and Exotic Materials,* edited by T. Matsubara and A. Kotani (Springer-Verlag, Berlin, 1994).
[2] U. Yaron *et al.,* Nature (London) **382**, 236 (1996).
[3] J. Schelten, G. Lippmann, and H. Ullmaier, J. Low Temp. Phys. **14**, 213 (1974).
[4] D. K. Christen, H. R. Kerchner, S. T. Sekula, and P. Thorel, Phys. Rev. B **21**, 102 (1980).
[5] B. K. Cho *et al.,* Phys. Rev. B **52**, 3684 (1995).
[6] R. J. Cava *et al.,* Nature (London) **367**, 252 (1994).
[7] J. Zarestky *et al.,* Phys. Rev. B **51**, 678 (1995).
[8] S. K. Sinha *et al.,* Phys. Rev. B **51**, 681 (1995).
[9] U. Yaron *et al.,* Phys. Rev. Lett. **73**, 2748 (1994).
[10] P. L. Gammel *et al.,* Phys. Rev. Lett. **59**, 2592 (1987).
[11] A. L. Fetter and P. C. Hohenber, in *Superconductivity,* edited by R. D. Parks (Marcel-Dekker, New York, 1969).
[12] K. Takanaka, Prog. Theor. Phys. **46**, 1301 (1971).
[13] V. Kogan *at al.,* Phys. Rev. B (to be published).
[14] S. L. Bud'ko (private communication).
[15] S. Oxx *et al.,* Physica (Amsterdam) **264C**, 103 (1996).